Title

Enhancing antibody responses by multivalent antigen display on thymus-independent DNA origami scaffolds

Authors

Eike-Christian Wamhoff[1, *], Larance Ronsard[2, *], Jared Feldman[2, *], Grant A. Knappe[1,3, *], Blake M. Hauser[2, *] Anna Romanov[1,4], Evan Lam[2], Kerri St. Denis[2], Julie Boucau[2], Amy K Barczak[2], Alejandro B. Balazs[2], Aaron Schmidt[2,5 **], Daniel Lingwood[2, **] and Mark Bathe[1,6,7, **]

[1]Department of Biological Engineering, Massachusetts Institute of Technology, Cambridge, MA 02139, United States

[2]Ragon Institute of Massachusetts General Hospital, Massachusetts Institute of Technology and Harvard University, Cambridge, MA 02139, United States

[3]Department of Chemical Engineering, Massachusetts Institute of Technology, Cambridge, MA 02139, United States

[4]Koch Institute for Integrative Cancer Research, Massachusetts Institute of Technology, Cambridge, MA 02139, United States

[5]Department of Microbiology, Harvard Medical School, Boston, MA 02115, United States

[6]Broad Institute of MIT and Harvard, Cambridge, MA 02139, United States

[7]Harvard Medical School Initiative for RNA Medicine, Harvard Medical School, Boston, MA 02115, United States

*These authors contributed equally

**Correspondence to: mark.bathe@mit.edu, dlingwood@mgh.harvard.edu or aschmidt@crystal.harvard.edu

Abstract

Multivalent antigen display is a well-established principle to enhance humoral immunity. Protein-based virus-like particles (VLPs) are commonly used to spatially organize antigens. However,

protein-based VLPs are limited in their ability to control valency on fixed scaffold geometries and are thymus-dependent antigens that elicit neutralizing B cell memory themselves, which can distract immune responses. Here, we investigated DNA origami as an alternative material for multivalent antigen display in vivo, applied to the receptor binding domain (RBD) of SARS-CoV-2 that is the primary antigenic target of neutralizing antibody responses. Icosahedral DNA-VLPs elicited neutralizing antibodies to SARS-CoV-2 in a valency-dependent manner following sequential immunization in mice, quantified by pseudo- and live-virus neutralization assays. Further, induction of B cell memory against the RBD required T cell help, but the immune sera did not contain boosted, class-switched antibodies against the DNA scaffold. This contrasted with protein-based VLP display of the RBD that elicited B cell memory against both the target antigen and the scaffold. Thus, DNA-based VLPs enhance target antigen immunogenicity without generating off-target, scaffold-directed immune memory, thereby offering a potentially important alternative material for particulate vaccine design.

Introduction

Multivalent display of antigens on virus-like particles (VLPs) can markedly improve the immunogenicity of subunit vaccines[1-3]. Nanoparticulate vaccines with diameters between 20 and 200 nm ensure efficient trafficking to secondary lymphoid organs, and particle diameters below 50 nm mitigate undesired retention at the injection site and promote the penetration of B cell follicles[4,5]. In secondary lymphoid organs, multivalency promotes B cell receptor (BCR) crosslinking and signaling as well as BCR-mediated antigen uptake, thereby driving B cell activation and humoral immunity[6-13].

The importance of BCR signaling for the generation of antibody responses was initially recognized for thymus-independent (TI) antigens, particularly of the TI-2 class[14-16]. The multivalent display of these non-protein antigens induces BCR crosslinking in the absence of T cell help. The resultant antibody responses proceed through extrafollicular B cell pathways, with limited germinal center (GC) reactions, affinity maturation, and induction of B cell memory[17,18]. Multivalent antigen display also enhances BCR-mediated responses to thymus-dependent (TD) antigens, namely proteins[8,9]. In this context, follicular T cell help enables GC reactions to generate affinity-matured B cell memory that can be boosted or recalled upon antigen reexposure[19-21]. Consequently, the nanoscale organization of antigens represents a well-established vaccine design principle not only for TI antigens, but also to elicit humoral immunity through the TD pathway[1-3].

60 Leveraging this design principle, protein-based virus-like particles (P-VLPs) have
61 emerged as an important material platform for multivalent subunit vaccines[22-38]. P-VLPs enable
62 the rigid display of TD antigens and have been used to investigate the impact of valency on B cell
63 activation in vivo, suggesting early B cell activation and downstream humoral immune responses
64 are improved substantially for some antigens as valency increases[8-10]. However, control over
65 antigen valency in P-VLPs is constrained to the constituent self-assembled protein scaffold
66 subunits, rendering the investigation of antigen valency on humoral immunity challenging without
67 simultaneously altering scaffold size, geometry, and protein composition[9,10]. Alternatively, if a
68 constant protein scaffold geometry is used, then current approaches are limited to stochastically-
69 controlled antigen valency and spatial positioning[8,29,30,38]. Further, protein-based scaffolds are TD
70 antigens that elicit humoral immunity themselves[38-40]. This potentially distracts antibody
71 responses from the target antigens of interest[41,42] , and might also lead to immune imprinting[43] or
72 original antigenic sin (OAS)[44,45] in which off-target, immunodominant epitopes distract from target
73 epitopes of interest in generating B cell memory. Finally, scaffold-directed immunological memory
74 may also result in antibody-dependent clearance of the vaccine material, thereby limiting
75 sequential or diversified immunizations with a given P-VLP [46,47].

76 To overcome these limitations of protein-based materials, here we sought to design rigid,
77 TI scaffolds of fixed geometry and size to display target TD antigens of varying valency. Fixing
78 scaffold geometry would isolate the impact of valency on promoting antibody responses, whereas
79 use of a TI scaffold would promote focusing of the antibody response on the target, TD antigen
80 of interest while confining scaffold-directed B cell responses to the non-boostable, TI pathway
81 that is devoid of immunological memory[48,49]. This approach may therefore avoid the off-target,
82 distracting antibody responses that affect P-VLPs[40,50] while retaining the ability to enhance
83 humoral immunity through multivalent antigen display. Wireframe DNA origami provides unique
84 access to such rationally designed VLPs of the optimal 50 nm size-scale, with scaffold-
85 independent control over valency of antigen display[51-56]. While we and others have leveraged this
86 DNA-based material platform in vitro to probe the nanoscale parameters of IgM recognition[57] and
87 BCR signaling in reporter B cell lines[58], the functional properties of this material remained to be
88 investigated in vivo where complex processes including particle trafficking, T cell help, and
89 scaffold degradation mediated by endonucleases are present.

90 To investigate the ability of these materials to elicit functional immune responses in vivo,
91 DNA-VLPs functionalized with the SARS-CoV-2 receptor binding domain (RBD) derived from the
92 spike glycoprotein, a key target for eliciting neutralizing antibodies against the virus[59-62], were

93 fabricated with varying valency, validated in vitro, and subsequently evaluated in vivo. This
94 nanoparticulate vaccine displayed enhanced binding to ACE2-expressing cells in vitro, and
95 induced BCR signaling in a valency-dependent manner in vitro consistent with previous
96 findings[58,63,64]. Following sequential vaccine immunizations in mice, we observed valency-
97 dependent enhancement of RBD-specific IgG responses and B cell memory recall in vivo using
98 this DNA-based scaffold material. Functionally, neutralization of the wildtype, Wuhan strain of
99 SARS-CoV-2 was found to be more efficient for antibodies elicited by DNA-VLPs compared with
100 those elicited by monomeric RBD alone. However, immunized sera did not contain boosted, DNA-
101 specific antibodies, and antibody enhancement was not observed in *Tcra*$^{-/-}$ mice, demonstrating
102 that boosting of RBD-specific antibodies went through the TD pathway even though antigens were
103 presented on TI scaffolds. This contrasted with a commonly used protein-based vaccine scaffold
104 that generated and boosted specific B cell memory to both the target, RBD antigen, and the
105 scaffold protein material. Taken together, our findings suggest that DNA origami-based materials
106 can be used to enhance humoral immunity in vivo using multivalent antigen display via focusing
107 of antibody responses on target antigens without the generation of distracting B cell memory
108 against the VLP scaffold itself.

109 Results and Discussion

110 SARS-CoV-2 displays trimeric spike glycoproteins on a ~100 nm diameter scaffold[65],
111 where each glycoprotein monomer contains the receptor-binding domain (RBD) for engaging the
112 ACE2 receptor mediating viral uptake, thereby rendering RBD a key target for neutralizing
113 antibody responses[59-62]. To ensure optimal trafficking of our vaccine platform, which requires
114 particle diameters smaller than 50 nm[5], we computationally designed and fabricated an
115 icosahedral DNA-VLP with 30 conjugation sites and approximately 34 nm scaffold diameter to
116 display the RBD[52,54]. A covalent *in situ* functionalization strategy employing strain-promoted azide-
117 alkyne cycloaddition (SPAAC) chemistry was used to ensure rigid, irreversible antigen attachment
118 to the DNA scaffold (**Figure 1A**)[53], unlike previous work that used a reversible, hybridization
119 strategy[58]. Towards this end, we synthesized 30 oligonucleotide staples bearing triethylene glycol
120 (TEG)-DBCO groups at their 5' ends to assemble DNA-VLPs symmetrically displaying 1x, 6x or
121 30x DBCO groups on their exterior (**Figure S1**, **Table S1 to S3**). Employing a reoxidation strategy,
122 the monomeric RBD was selectively modified at an engineered C-terminal Cys with an SMCC-
123 TEG-azide linker to yield RBD-Az which was subsequently incubated with DBCO-bearing DNA
124 origami to fabricate **I52-1x, -6x,** and **-30x** (**Figures 1B and S2**, **Note S1**). The optimization of
125 reaction conditions yielded near-quantitative functionalization efficiency of conjugation sites as

126 determined by denaturing, reversed-phase HPLC[53] and Trp fluorescence[58] (**Figures 1C and S3**).
127 The monodispersity of purified DNA-VLPs was validated by dynamic light scattering (DLS)
128 (**Figure 1D**). Analysis of **I52-30x** via negative-strain transmission electron microscopy (TEM)
129 validated structural integrity of the DNA origami with the desired total size of approximately 45 nm
130 (**Figure 1E and S4**). While the icosahedral geometry could not be fully resolved, presumably due
131 to accumulation of uranyl formate in the interior of the DNA origami, antigens were clearly visible
132 and organized symmetrically.

133 To investigate the binding activity of RBD-Az before and after conjugation to DNA-VLPs,
134 we conducted flow cytometry experiments with ACE2-expressing HEK293 cells (**Figure 2A**).
135 Initially, monovalent binding of wild-type RBD and fluorophore-labeled RBD-Cy5, obtained by
136 selectively labeling the azide, was compared (**Figure 2B and C**). The RBD constructs were
137 incubated at 200 nM with the HEK293 cells and bound antigen was detected using the previously
138 described anti-RBD antibody CR3022[62]. These experiments revealed comparable binding
139 between the two constructs, demonstrating preservation of binding activity of the receptor binding
140 motif (RBM) in RBD and the viability of the reoxidation strategy for selective labeling of the
141 terminal Cys (**Figure S2, Note S1**).

142 Next, we explored whether multivalent RBD display using DNA-VLPs would result in
143 increased avidity. Two additional fluorophore-labeled DNA-VLPs, **I52-Cy5-30x** and **I52-Cy5**, were
144 fabricated to allow for direct detection of binding (**Figure 1B and S1**). Binding of **I52-Cy5-30x** was
145 significantly enhanced compared to monomeric RBD-Cy5, while no binding was observed for the
146 **I52-Cy5** (**Figure 2D and 2E**). When correcting for Cy5 brightness per RBD, **I52-Cy5-30x**
147 displayed approximately one order of magnitude higher median fluorescence intensity compared
148 with monomeric RBD-Cy5, likely due to avidity effects in multivalent DNA-VLP binding to the
149 cognate ACE2 receptor.

150 We then evaluated the impact of RBD-functionalized DNA-VLPs on BCR signaling using
151 a previously described Ca^{2+} flux assay (**Figure 2A**)[63]. Specifically, Ramos B cell lines expressing
152 the somatic CR3022 or B38 antibodies were established[62,66] and BCR signaling was validated by
153 incubation with anti-IgM antibody. At 30 nM antigen concentration, monomeric RBD did not elicit
154 B cell activation in vitro (**Figure 2F and 2G**). In contrast, incubation of the Ramos B cells with
155 multivalent DNA-VLPs at the same antigen concentration resulted in efficient BCR signaling. We
156 further observed valency-dependent increases in total Ca^{2+} flux for both cell lines with **I52-30x**
157 more potent than **I52-6x**. CR3022 (K_D = 0.27 μM, **Figure 2F**) and B38 (K_D = 1.00 μM, **Figure 2G**)
158 bind distinct RBD epitopes with moderate monovalent affinity as reported for the corresponding

159 Fab fragments[67]. Despite this four-fold difference in affinity, we observed comparable total BCR
160 signaling relative to the IgM control for all functionalized DNA-VLPs, consistent with previously
161 described avidity effects at the B cell surface[68]. We thereby concluded that our DNA-VLPs
162 efficiently bound and induced signaling by RBD-specific BCRs in a valency-dependent manner,
163 analogous to previous studies using similar assays to evaluate protein- and DNA-scaffolded
164 multivalent subunit vaccines[58,63,64,69-74].

165 To investigate whether RBD-functionalized DNA-VLPs activated B cells in vivo to induce
166 antibody responses, C57BL/6 mice were sequentially immunized intraperitoneally with
167 monomeric RBD, **I52-6x,** or **I52-30x** at doses equivalent to 7.5 µg RBD with Sigma adjuvant
168 (**Figure 3A and S3**). Serum IgG responses against the RBD were monitored throughout this
169 regimen using ELISA and correlated with in vitro BCR signaling findings (**Figure 3B and S5**).
170 Following boost 1, we observed an approximately 130-fold increase in endpoint dilutions for **I52-**
171 **30x** over monomeric RBD. In contrast, **I52-6x** elicited comparable antibody responses with
172 respect to monomeric RBD following each boost, suggesting that a higher minimum antigen copy
173 number is needed to enhance B cell responses in vivo compared with in vitro (**Figure 2F and**
174 **2G**), which may be due to differences in trafficking or degradation rates, for example, between
175 **I52-6x** and **I52-30x**. Overall, IgG titers increased for monomeric RBD, **I52-6x**, and **I52-30x**
176 following boost 2, converging to similar endpoint dilutions. These findings of earlier and stronger
177 boosting of IgG titers and efficient B cell memory recall elicited by the **I52-30x** are hallmarks of
178 multivalent versus monomeric subunit vaccines[23,24], consistent with enhanced IgG titers elicited
179 by P-VLPs of increasing valency[8-10].

180 To quantify the quality of antibody responses generated by DNA-VLPs, valency-
181 dependent enhancement of RBD-specific antibody responses was interrogated using viral
182 neutralization assays (**Figure 3C, 3D and S6**). In both pseudo- and native virus neutralization
183 assays, efficient neutralization of the wild-type, Wuhan strain of SARS-CoV-2 resulted from DNA-
184 VLPs. However, across both the pseudo- and native virus assays, **I52-30x** elicited IgG titers with
185 significantly higher neutralization potency compared with both monomeric RBD and **I52-6x**,
186 indicating that the higher valency, 30x-RBD DNA-VLP produced significantly superior quality
187 antibodies, which have been correlated with improved patient outcomes[75-77].

188 To confirm that the boosted, RBD-specific IgG titers were achieved via the TD route, we
189 compared the same sequential immunization regime in wild-type C57BL/6 versus *Tcra*$^{-/-}$ mice
190 that lack functional TCRs[78] (**Figure 3A**). **I52-30x** elicited robust IgM responses in both genotypes,

191 whereas RBD-specific IgG titers were not boosted in *Tcra*$^{-/-}$ mice (**Figure 3E**). Hence, IgG
192 boosting following sequential immunization with DNA-VLPs was due to TD, or T cell dependent,
193 recall of B cell memory.

194 To contrast our findings on DNA-VLPs with protein-based materials, we employed ferritin-
195 based P-VLPs with 24-valent display of RBDs (**P-VLP-24x**) on a scaffold of approximately 12 nm
196 scaffold diameter (**Figure S1**)[32,39]. Following the validation of efficient B cell activation in vitro
197 (**Figure S7**), C57BL/6 mice were sequentially immunized intraperitoneally with monomeric wild-
198 type RBD, **I52-30x**, or **P-VLP-24x** at doses equivalent to 7.5 µg RBD (**Figure 4A**). While RBD-
199 specific IgG titers were enhanced for both **I52-30x** and **P-VLP-24x** (**Figure 4B and 4C**), **P-VLP-**
200 **24x** also exhibited boosted IgG titers against the ferritin protein scaffold itself (**Figure 4B**). In
201 contrast, we did not observe boosting of DNA-specific IgG titers following immunization with DNA-
202 VLPs, indicating an absence of B cell memory of the DNA-based scaffold (**Figure 4C and S8**).
203 Importantly, this same behavior was observed when a higher DNA dose was administered (**I52-**
204 **6x**) and also when monomeric RBD was administered (**Figure S8**).

205 Conclusions

206 Rational vaccine design seeks to leverage multivalent antigen display together with
207 epitope-focusing to generate potent, neutralizing antibody responses[79]. P-VLPs have
208 demonstrated limited control over antigen valency and antigen type[8,9,29,38] together with low-cost,
209 scalable production[27,30,32,38], but they suffer from the generation of distracting, off-target antibody
210 responses against the protein scaffold material itself[39,40,50].

211 As an alternative VLP scaffold material, here we investigated the multivalent display of the
212 RBD antigen from SARS-CoV-2 using icosahedral DNA origami VLPs. Our results suggest that
213 DNA-VLPs covalently functionalized with 30 copies of the RBD antigen significantly enhance
214 neutralizing antibody responses compared with monomeric RBD antigen alone, consistent with
215 findings for P-VLPs displaying RBD[10,30,32,33,38,39] , as well as other antigens[8,9,23]. However, unlike
216 P-VLPs that elicit scaffold-directed humoral immunity within the memory compartment[32,33,38,39],
217 compatible with our findings here for a ferritin-based P-VLP, DNA-VLPs did not generate B cell
218 memory to the VLP scaffold material itself. Importantly, this suggests that the distraction of
219 antibody responses away from the target protein antigen of interest in P-VLPs, which may reduce
220 cross-neutralization of variants in the case of SARS-CoV-2[39] and potentially result in irreversible
221 off-target immune imprinting[43,44,45,80], may be avoided by DNA-VLPs. While our finding was
222 expected for TI antigens such as DNA, it is also well established that TD antibody responses can

223 be generated for TI antigens covalently attached to protein scaffolds[81,82]. Our results, however,
224 indicate that the inverse is not necessarily the default, namely scaffolding TD antigens with TI
225 antigens does not generate boostable B cell memory against the TI scaffold for our vaccine
226 platform. At the same time, we observed robust valency-dependent TD antibody responses to the
227 RBD, akin to virosomal and ISCOM-based vaccine designs in which protein antigens are
228 multivalently displayed by TI antigen-composed matrices[83-86].

229 Because DNA origami uniquely offers simultaneous yet independent control over spatial
230 antigen display, scaffold size, and scaffold geometry, we were able to investigate the impact of
231 antigen valency alone on antibody responses using an optimally sized, geometrically fixed ~35
232 nm icosahedral VLP scaffold, whereby 30 but not six copies of RBD were found to be sufficient
233 to enhance neutralizing antibody titers compared with monomeric RBD alone. Future work may
234 seek to additionally examine the impact of antigen spacing with fixed valency[58], as well as
235 alternative scaffold sizes and geometries, which might ultimately be required to resolve critical
236 thresholds for enhancing antibody responses beyond monomeric antigens, as well as to optimize
237 B cell responses for certain antigens[9,29,30]. Additional important extensions to our study include
238 examining GC formation in B cell follicles, which is known to be important to generate broadly
239 neutralizing antibodies and long-lived humoral immunity[87-89] . Toward this end, it will be interesting
240 to investigate to what extent multivalent antigen display by DNA-VLPs is maintained in secondary
241 lymphoid organs, particularly in the presence of endonuclease[90,91] and protease[89] degradation;
242 what the breadth of neutralizing antibody responses is; and what the longevity of humoral
243 immunity is. To further enhance B cell activation and trafficking to secondary lymphoid organs,
244 DNA-VLP valency may be increased, slow escalating dosing may be used[92], and active follicle
245 targeting with carbohydrates may be incorporated[5,87]. Co-formulation with TLR-based adjuvants
246 may also be used to enhance T cell help, drive GC reactions, and improve humoral immunity[93-95].
247 Finally, DNA stabilization strategies[91] may be needed to increase the longevity of DNA-VLPs
248 within follicles and GCs in the presence of endonucleases.

249 Beyond rational vaccine design and promoting antibody focusing, our discovery that DNA
250 scaffolds are not neutralized by DNA-specific antibodies is of significant importance towards
251 enabling redosing in therapeutic nucleic acid delivery by avoiding antibody-dependent
252 clearance[46,47], whereby DNA origami may offer an important delivery vector[96].

253 Methods

254 Methods are described in the **Supporting Information**.

Acknowledgments

E.-C.W., G.K., and M.B. were supported by NIH R21-EB026008, NSF CCF-1564025, CBET-1729397, and CCF-1956054, ONR N00014-21-1-4013 and N00014-17-1-2609, ARO ISN W911NF-13-D-0001, and Fast Grants Agreement EFF 4/15/20. E.-C. W. was additionally supported by the Feodor Lynen Fellowship of the Alexander von Humboldt Foundation. B.M.H was supported by NIGMS (T32GM007753) and F30 AI160908. J.F. was supported by NIGMS (T32AI007245). A.G.S. was supported by NIH (R01 AI146779) and a Massachusetts Consortium on Pathogenesis Readiness (MassCPR) grant. D.L was supported by NIH (R01AI124378, R01AI153098, R01AI155447, U19AI057229, P30AI060354). The SARS-CoV-2 virus work was performed at the Ragon Institute's Biosafety Level 3 facility, which is supported by the NIH-funded Harvard University Center for AIDS Research (P30 AI060354) and the Massachusetts Consortium on Pathogen Readiness (MassCPR).

Competing interests

The Massachusetts Institute of Technology has filed a patent (US application number 16/752,394) covering the use of DNA origami as a vaccine platform on behalf of the co-inventors (E.-C. W. and M. B.).

Data availability

The DNA sequences used to assemble the wireframe DNA origami are included in Tables S1-3. All data files used to generate the figures in this manuscript are available from A. S., D. L. or M. B. upon request.

Software and code availability

No previously unreported code or software were used for data collection and analysis.

Figures

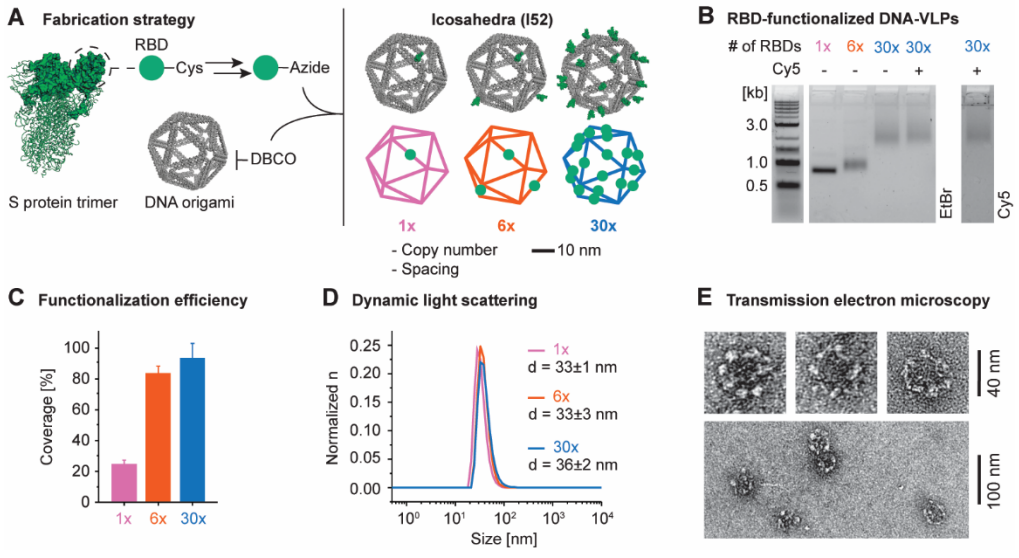

Figure 1. Design and synthesis of DNA-VLPs covalently displaying the SARS-CoV-2 RBD.

(A) Recombinant RBD bearing an additional Cys residue at the C-terminus was expressed. The C-terminal Cys was selectively labeled with and SMCC-TEG-azide linker and subsequently conjugated to DBCO-bearing DNA-VLPs. The icosahedral DNA origami objects of approximately 50 nm diameter displaying 1, 6 and 30 copies of the RBD were fabricated. **(B)** Agarose gel electrophoresis (AGE) shows the gel shift due to increasing RBD copy number as well as low polydispersity of the VLPs samples after purification. An additional VLP bearing 5 copies of Cy5 was produced for ACE2-binding flow cytometry experiments. **(C)** The coverage of the DNA-VLPs with RBD was quantified via Trp fluorescence. **(D)** Dynamic light scattering (DLS) was used to assess the dispersity of functionalized VLP samples. Representative histograms are shown**. (E)** Transmission electron micrographs (TEM) of **I52-30x** were obtained by negative staining using 2% uranyl formate and validate the symmetric nanoscale organization of antigens. Coverage values were determined from n = 3 biological replicates for **I52-1x** and from n = 6 biological replicates for **I52-6x** and **I52-30x**. Diameters were determined from 3 technical replicates. Error bars represent the standard error of the mean.

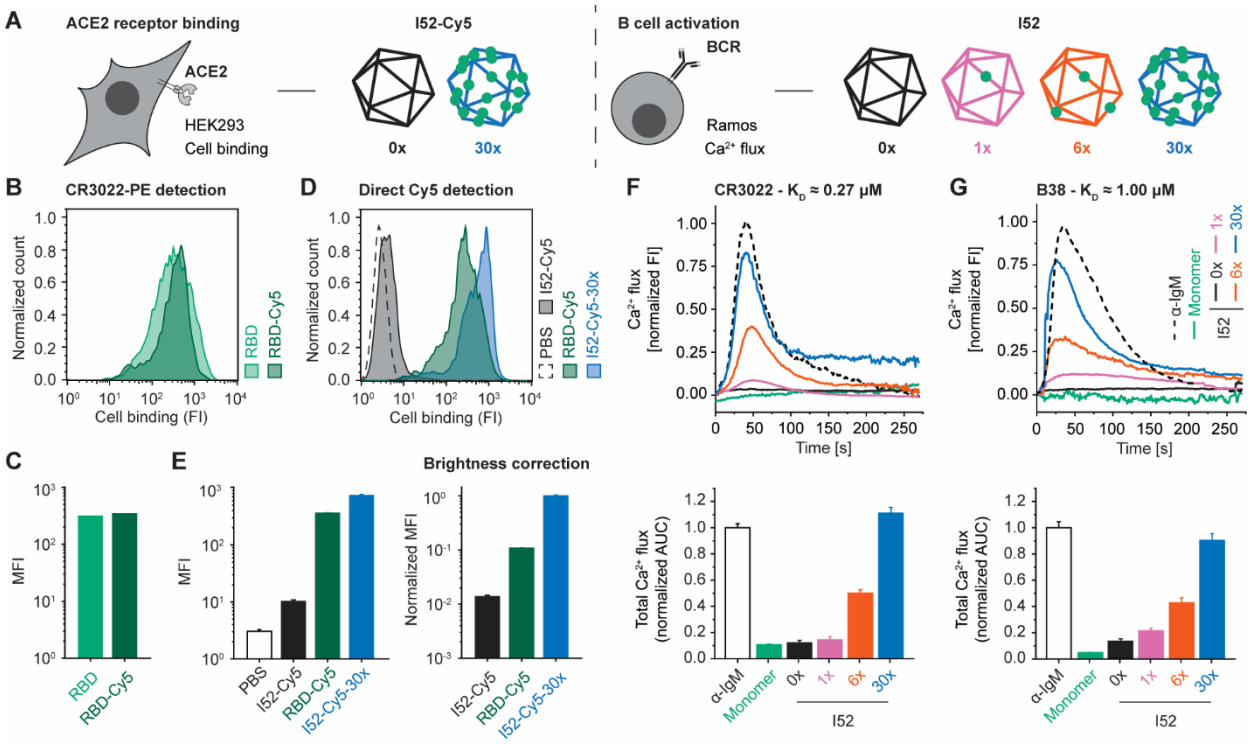

Figure 2. In vitro activity of RBD-functionalized DNA-VLPs.

(A) An overview of the in vitro activity assays and corresponding DNA-VLPs is shown. **(B and C)** ACE2-expressing HEK293 cells were incubated with 200 nM RBD. Binding was detected in flow cytometry experiments using PE-labeled CR3022 and a PE-labeled secondary antibody, demonstrating preserved binding activity for chemically modified RBD-Cy5 compared to wild-type RBD. **(D and E)** Incubation with Cy5-labeled **I52-Cy5-30x** at 100 nM RBD revealed enhanced binding compared to RBD-Cy5 due to multivalency effects. No unspecific binding for non-functionalized **I52-Cy5** was observed. The brightness of Cy5-labeled **I52-Cy5-30x** (5 Cy5 per 30 RBDs) and RBD-Cy5 (1 Cy5 per 1 RBD) was quantified experimentally (**Figure S4**) and MFI values were corrected accordingly. **(F and G)** Ramos B cells expressing the BCRs C3022 and B38 were incubated with α-IgM, wild-type RBD or RBD-functionalized DNA-VLPs at 30 nM RBD. Ca^{2+} flux in response to RBD incubation was assayed using Fura Red. Representative fluorescence intensity curves are shown (top). Total Ca^{2+} flux was quantified via the normalized AUC, revealing robust activation of BCR-expressing Ramos B cells by functionalized DNA-VLPs (bottom). No stimulation was observed for wild-type RBD or for non-functionalized **I52-0x**. Representative histograms are shown for ACE2 binding assays and MFI values were determined from n = 3 biological replicates. Normalized AUC values were determined from n = 3 biological replicates. Error bars represent the standard error of the mean.

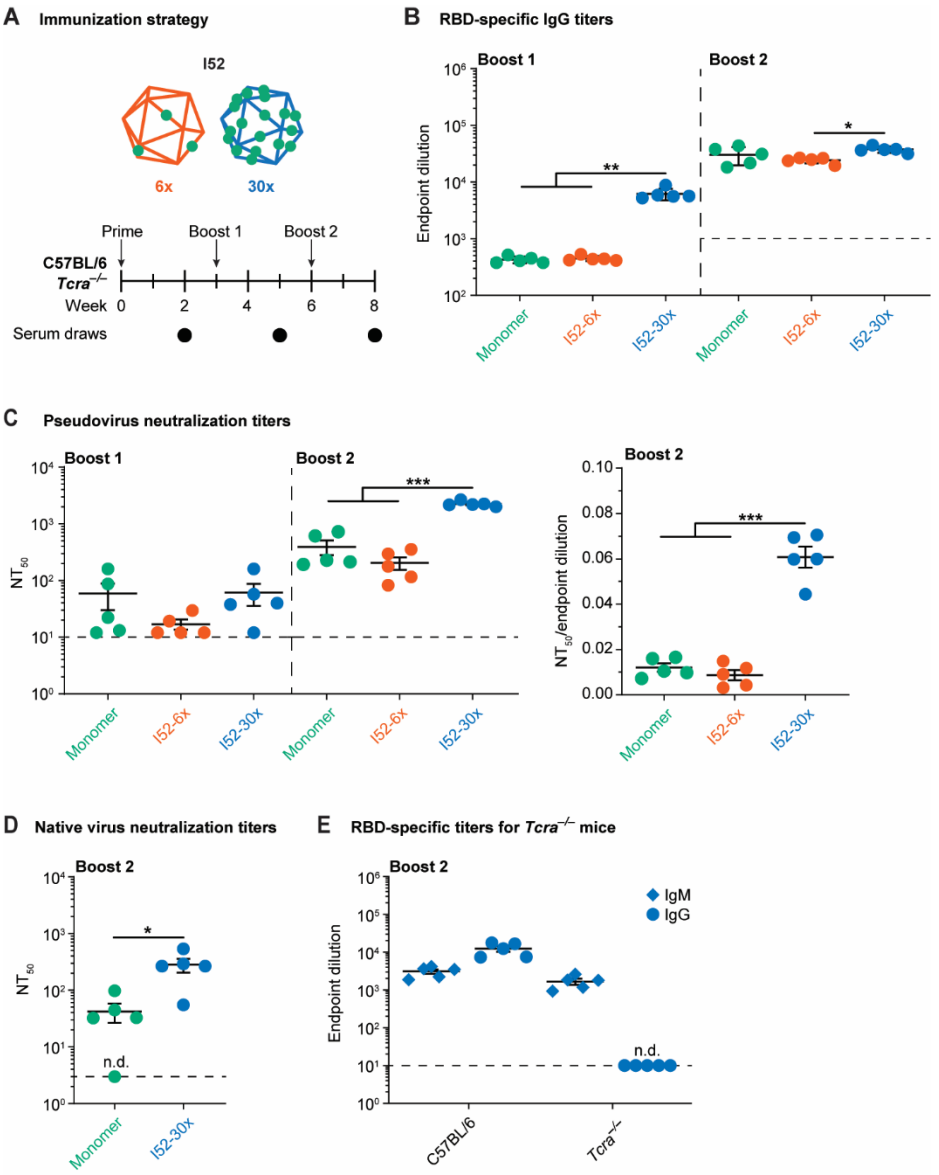

Figure 3. RBD-specific antibody responses to functionalized DNA-VLPs.

(A) Mice were sequentially immunized with monomeric RBD and RBD-functionalized DNA-VLPs of varying copy number. **(B)** RBD-specific IgG endpoint dilutions revealed enhanced antibody responses for **I52-30x** compared to both monomeric RBD and **I52-6x**. **(C)** Serum neutralization titers expressed as NT_{50} values against pseudoviruses modeling the wild-type, Wuhan strain**. (D)** Neutralization of native Wuhan SARS-CoV-2**. (E)** IgM and IgG titers of RBD-specific antibodies elicited in *Tcra*$^{-/-}$ and wild-type mice after sequential immunization with **I52-30x.** N=5 animals were used in each experimental group. One-way ANOVA was performed followed by Dunnett's T3 multiple comparison test at α = 0.05 for **(B)** and **(C)**. Welch's t-test was performed at α = 0.05 for **(D).** Error bars represent the standard error of the mean. Non-responder mice (denoted as n.d. = not detectable) were not considered for statistical analysis.

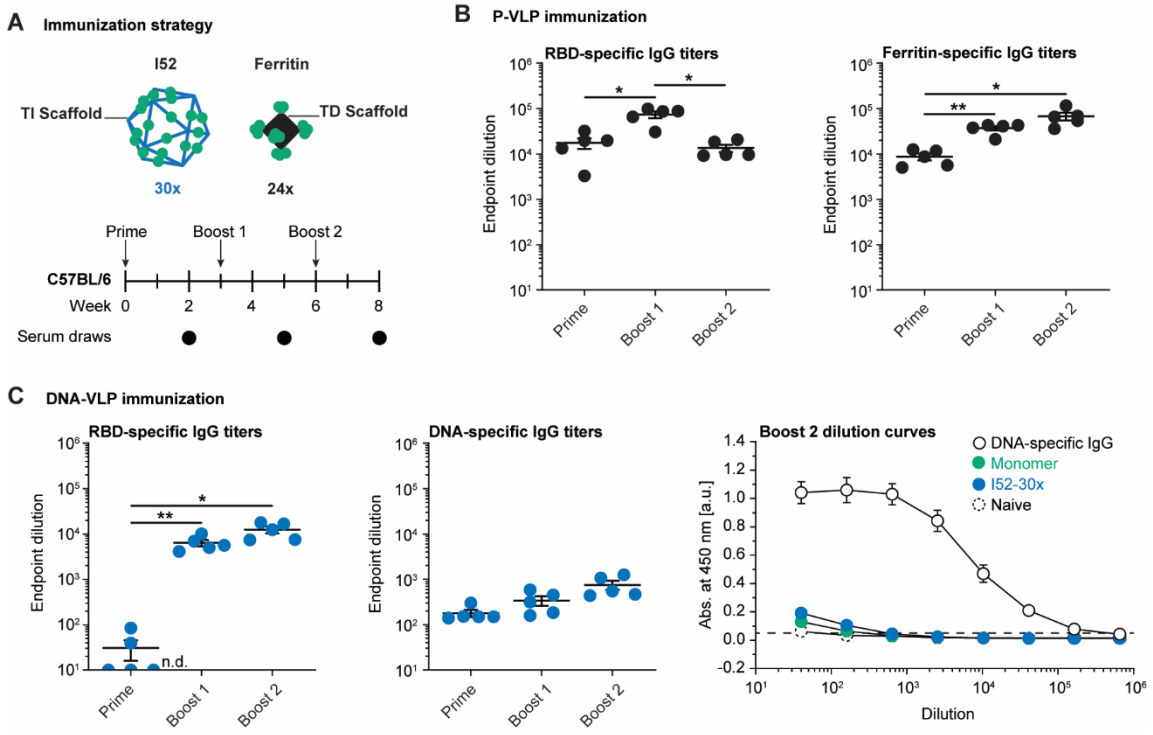

Figure 4. Scaffold-specific antibody responses to functionalized DNA-VLPs and P-VLPs.

(A) Mice were sequentially immunized with monomeric RBD, RBD-functionalized DNA-VLP, or ferritin-based P-VLP. **(B)** RBD-specific and scaffold-specific IgG endpoint dilutions for the P-VLP immunization. **(C)** RBD-specific and scaffold-specific IgG endpoint dilutions for the DNA-VLP immunization; dilution curves for Boost 2 of the DNA-specific ELISA. The DNA-specific IgG control was diluted from 10 µg/ml. N=5 animals were used in each experimental group. One-way ANOVA was performed followed by Dunnett's T3 multiple comparison test at $\alpha = 0.05$. Error bars represent the standard error of the mean. Non-responder mice (denoted as n.d. = not detectable) were not considered for statistical analysis.

References

1 Singh, A. Eliciting B cell immunity against infectious diseases using nanovaccines. *Nat Nanotechnol* **16**, 16-24, doi:10.1038/s41565-020-00790-3 (2021).

2 Nguyen, B. & Tolia, N. H. Protein-based antigen presentation platforms for nanoparticle vaccines. *NPJ Vaccines* **6**, 70, doi:10.1038/s41541-021-00330-7 (2021).

3 Irvine, D. J. & Read, B. J. Shaping humoral immunity to vaccines through antigen-displaying nanoparticles. *Curr Opin Immunol* **65**, 1-6, doi:10.1016/j.coi.2020.01.007 (2020).

4 Zhang, Y. N. *et al.* Nanoparticle Size Influences Antigen Retention and Presentation in Lymph Node Follicles for Humoral Immunity. *Nano Lett* **19**, 7226-7235, doi:10.1021/acs.nanolett.9b02834 (2019).

5 Yousefpour, P., Ni, K. & Irvine, D. J. Targeted modulation of immune cells and tissues using engineered biomaterials. *Nature Reviews Bioengineering* **1**, 107-124, doi:10.1038/s44222-022-00016-2 (2023).

6 Batista, F. D., Iber, D. & Neuberger, M. S. B cells acquire antigen from target cells after synapse formation. *Nature* **411**, 489-494, doi:10.1038/35078099 (2001).

7 Abbott, R. K. *et al.* Precursor Frequency and Affinity Determine B Cell Competitive Fitness in Germinal Centers, Tested with Germline-Targeting HIV Vaccine Immunogens. *Immunity* **48**, 133-146 e136, doi:10.1016/j.immuni.2017.11.023 (2018).

8 Marcandalli, J. *et al.* Induction of Potent Neutralizing Antibody Responses by a Designed Protein Nanoparticle Vaccine for Respiratory Syncytial Virus. *Cell* **176**, 1420-1431 e1417, doi:10.1016/j.cell.2019.01.046 (2019).

9 Kato, Y. *et al.* Multifaceted Effects of Antigen Valency on B Cell Response Composition and Differentiation In Vivo. *Immunity* **53**, 548-563 e548, doi:10.1016/j.immuni.2020.08.001 (2020).

10 He, L. *et al.* Single-component, self-assembling, protein nanoparticles presenting the receptor binding domain and stabilized spike as SARS-CoV-2 vaccine candidates. *Sci Adv* **7**, doi:10.1126/sciadv.abf1591 (2021).

11 Batista, F. D. & Harwood, N. E. The who, how and where of antigen presentation to B cells. *Nat Rev Immunol* **9**, 15-27, doi:10.1038/nri2454 (2009).

12 Kwak, K., Akkaya, M. & Pierce, S. K. B cell signaling in context. *Nat Immunol* **20**, 963-969, doi:10.1038/s41590-019-0427-9 (2019).

13 Gold, M. R. & Reth, M. G. Antigen Receptor Function in the Context of the Nanoscale Organization of the B Cell Membrane. *Annu Rev Immunol* **37**, 97-123, doi:10.1146/annurev-immunol-042718-041704 (2019).

14 Dintzis, H. M., Dintzis, R. Z. & Vogelstein, B. Molecular determinants of immunogenicity: the immunon model of immune response. *Proc Natl Acad Sci U S A* **73**, 3671-3675, doi:10.1073/pnas.73.10.3671 (1976).

15 Tittle, T. V. & Rittenberg, M. B. IgG B memory cell subpopulations: differences in susceptibility to stimulation by TI-1 and TI-2 antigens. *J Immunol* **124**, 202-206 (1980).

16 Obukhanych, T. V. & Nussenzweig, M. C. T-independent type II immune responses generate memory B cells. *J Exp Med* **203**, 305-310, doi:10.1084/jem.20052036 (2006).

17 Vinuesa, C. G. & Chang, P. P. Innate B cell helpers reveal novel types of antibody responses. *Nat Immunol* **14**, 119-126, doi:10.1038/ni.2511 (2013).

18 Cerutti, A., Cols, M. & Puga, I. Marginal zone B cells: virtues of innate-like antibody-producing lymphocytes. *Nat Rev Immunol* **13**, 118-132, doi:10.1038/nri3383 (2013).

19 Crotty, S. T Follicular Helper Cell Biology: A Decade of Discovery and Diseases. *Immunity* **50**, 1132-1148, doi:10.1016/j.immuni.2019.04.011 (2019).

20 Victora, G. D. & Nussenzweig, M. C. Germinal Centers. *Annu Rev Immunol* **40**, 413-442, doi:10.1146/annurev-immunol-120419-022408 (2022).

21 Cyster, J. G. & Allen, C. D. C. B Cell Responses: Cell Interaction Dynamics and Decisions. *Cell* **177**, 524-540, doi:10.1016/j.cell.2019.03.016 (2019).
22 Boyoglu-Barnum, S. *et al.* Quadrivalent influenza nanoparticle vaccines induce broad protection. *Nature* **592**, 623-628, doi:10.1038/s41586-021-03365-x (2021).
23 Kanekiyo, M. *et al.* Self-assembling influenza nanoparticle vaccines elicit broadly neutralizing H1N1 antibodies. *Nature* **499**, 102-106, doi:10.1038/nature12202 (2013).
24 Kanekiyo, M. *et al.* Rational Design of an Epstein-Barr Virus Vaccine Targeting the Receptor-Binding Site. *Cell* **162**, 1090-1100, doi:10.1016/j.cell.2015.07.043 (2015).
25 Kanekiyo, M. *et al.* Mosaic nanoparticle display of diverse influenza virus hemagglutinins elicits broad B cell responses. *Nat Immunol* **20**, 362-372, doi:10.1038/s41590-018-0305-x (2019).
26 Martinez-Murillo, P. *et al.* Particulate Array of Well-Ordered HIV Clade C Env Trimers Elicits Neutralizing Antibodies that Display a Unique V2 Cap Approach. *Immunity* **46**, 804-817 e807, doi:10.1016/j.immuni.2017.04.021 (2017).
27 Akahata, W. *et al.* A virus-like particle vaccine for epidemic Chikungunya virus protects nonhuman primates against infection. *Nat Med* **16**, 334-338, doi:10.1038/nm.2105 (2010).
28 Arunachalam, P. S. *et al.* Adjuvanting a subunit COVID-19 vaccine to induce protective immunity. *Nature* **594**, 253-258, doi:10.1038/s41586-021-03530-2 (2021).
29 Cohen, A. A. *et al.* Mosaic nanoparticles elicit cross-reactive immune responses to zoonotic coronaviruses in mice. *Science* **371**, 735-741, doi:10.1126/science.abf6840 (2021).
30 Cohen, A. A. *et al.* Mosaic RBD nanoparticles protect against challenge by diverse sarbecoviruses in animal models. *Science*, eabq0839, doi:10.1126/science.abq0839 (2022).
31 Dalvie, N. C. *et al.* Engineered SARS-CoV-2 receptor binding domain improves manufacturability in yeast and immunogenicity in mice. *Proc Natl Acad Sci U S A* **118**, doi:10.1073/pnas.2106845118 (2021).
32 King, H. A. D. *et al.* Efficacy and breadth of adjuvanted SARS-CoV-2 receptor-binding domain nanoparticle vaccine in macaques. *Proc Natl Acad Sci U S A* **118**, doi:10.1073/pnas.2106433118 (2021).
33 Joyce, M. G. *et al.* SARS-CoV-2 ferritin nanoparticle vaccines elicit broad SARS coronavirus immunogenicity. *Cell Rep* **37**, 110143, doi:10.1016/j.celrep.2021.110143 (2021).
34 Yassine, H. M. *et al.* Hemagglutinin-stem nanoparticles generate heterosubtypic influenza protection. *Nat Med* **21**, 1065-1070, doi:10.1038/nm.3927 (2015).
35 Jardine, J. G. *et al.* Priming a broadly neutralizing antibody response to HIV-1 using a germline-targeting immunogen. *Science* **349**, 156-161, doi:10.1126/science.aac5894 (2015).
36 Peabody, D. S. *et al.* Immunogenic display of diverse peptides on virus-like particles of RNA phage MS2. *J Mol Biol* **380**, 252-263, doi:10.1016/j.jmb.2008.04.049 (2008).
37 Moon, J. J. *et al.* Enhancing humoral responses to a malaria antigen with nanoparticle vaccines that expand Tfh cells and promote germinal center induction. *Proc Natl Acad Sci U S A* **109**, 1080-1085, doi:10.1073/pnas.1112648109 (2012).
38 Walls, A. C. *et al.* Elicitation of Potent Neutralizing Antibody Responses by Designed Protein Nanoparticle Vaccines for SARS-CoV-2. *Cell* **183**, 1367-1382 e1317, doi:10.1016/j.cell.2020.10.043 (2020).
39 Hauser, B. M. *et al.* Rationally designed immunogens enable immune focusing following SARS-CoV-2 spike imprinting. *Cell Rep* **38**, 110561, doi:10.1016/j.celrep.2022.110561 (2022).
40 Kraft, J. C. *et al.* Antigen- and scaffold-specific antibody responses to protein nanoparticle immunogens. *Cell Rep Med* **3**, 100780, doi:10.1016/j.xcrm.2022.100780 (2022).

41 Herzenberg, L. A., Tokuhisa, T. & Herzenberg, L. A. Carrier-priming leads to hapten-specific suppression. *Nature* **285**, 664-667, doi:10.1038/285664a0 (1980).
42 Chackerian, B., Durfee, M. R. & Schiller, J. T. Virus-like display of a neo-self antigen reverses B cell anergy in a B cell receptor transgenic mouse model. *J Immunol* **180**, 5816-5825, doi:10.4049/jimmunol.180.9.5816 (2008).
43 Wheatley, A. K. *et al.* Immune imprinting and SARS-CoV-2 vaccine design. *Trends Immunol* **42**, 956-959, doi:10.1016/j.it.2021.09.001 (2021).
44 Francis, T. On the Doctrine of Original Antigenic Sin. *Proc Am Philos Soc* **104**, 572-578 (1960).
45 Monto, A. S., Malosh, R. E., Petrie, J. G. & Martin, E. T. The Doctrine of Original Antigenic Sin: Separating Good From Evil. *J Infect Dis* **215**, 1782-1788, doi:10.1093/infdis/jix173 (2017).
46 Alonso-Padilla, J. *et al.* Development of Novel Adenoviral Vectors to Overcome Challenges Observed With HAdV-5-based Constructs. *Mol Ther* **24**, 6-16, doi:10.1038/mt.2015.194 (2016).
47 Zak, D. E. *et al.* Merck Ad5/HIV induces broad innate immune activation that predicts CD8(+) T-cell responses but is attenuated by preexisting Ad5 immunity. *Proc Natl Acad Sci U S A* **109**, E3503-3512, doi:10.1073/pnas.1208972109 (2012).
48 Lucas, C. R. *et al.* DNA Origami Nanostructures Elicit Dose-Dependent Immunogenicity and Are Nontoxic up to High Doses In Vivo. *Small* **18**, e2108063, doi:10.1002/smll.202108063 (2022).
49 Liu, X. *et al.* A DNA nanostructure platform for directed assembly of synthetic vaccines. *Nano Lett* **12**, 4254-4259, doi:10.1021/nl301877k (2012).
50 Olshefsky, A., Richardson, C., Pun, S. H. & King, N. P. Engineering Self-Assembling Protein Nanoparticles for Therapeutic Delivery. *Bioconjug Chem*, doi:10.1021/acs.bioconjchem.2c00030 (2022).
51 Rothemund, P. W. Folding DNA to create nanoscale shapes and patterns. *Nature* **440**, 297-302, doi:10.1038/nature04586 (2006).
52 Veneziano, R. *et al.* Designer nanoscale DNA assemblies programmed from the top down. *Science* **352**, 1534, doi:10.1126/science.aaf4388 (2016).
53 Knappe, G. A., Wamhoff, E. C., Read, B. J., Irvine, D. J. & Bathe, M. In situ covalent functionalization of DNA origami virus-like particles. *ACS Nano* **15**, 14316-14322, doi:10.1021/acsnano.1c03158 (2021).
54 Jun, H. *et al.* Rapid prototyping of arbitrary 2D and 3D wireframe DNA origami. *Nucleic Acids Res* **49**, 10265-10274, doi:10.1093/nar/gkab762 (2021).
55 Wamhoff, E. C. *et al.* Programming structured DNA assemblies to probe biophysical processes. *Annu Rev Biophys* **48**, 395-419, doi:10.1146/annurev-biophys-052118-115259 (2019).
56 Knappe, G. A., Wamhoff, E. C. & Bathe, M. Functionalizing DNA origami to investigate and interact with biological systems. *Nat Rev Mater* **8**, 123-138, doi:10.1038/s41578-022-00517-x (2023).
57 Shaw, A. *et al.* Binding to nanopatterned antigens is dominated by the spatial tolerance of antibodies. *Nat Nanotechnol* **14**, 184-190, doi:10.1038/s41565-018-0336-3 (2019).
58 Veneziano, R. *et al.* Role of nanoscale antigen organization on B-cell activation probed using DNA origami. *Nat Nanotechnol* **15**, 716-723, doi:10.1038/s41565-020-0719-0 (2020).
59 Dai, L. & Gao, G. F. Viral targets for vaccines against COVID-19. *Nat Rev Immunol* **21**, 73-82, doi:10.1038/s41577-020-00480-0 (2021).
60 Kleanthous, H. *et al.* Scientific rationale for developing potent RBD-based vaccines targeting COVID-19. *NPJ Vaccines* **6**, 128, doi:10.1038/s41541-021-00393-6 (2021).

61 Walls, A. C. *et al.* Structure, Function, and Antigenicity of the SARS-CoV-2 Spike Glycoprotein. *Cell*, doi:10.1016/j.cell.2020.02.058 (2020).
62 Yuan, M. *et al.* A highly conserved cryptic epitope in the receptor binding domains of SARS-CoV-2 and SARS-CoV. *Science* **368**, 630-633, doi:10.1126/science.abb7269 (2020).
63 Weaver, G. C. *et al.* In vitro reconstitution of B cell receptor-antigen interactions to evaluate potential vaccine candidates. *Nat Protoc* **11**, 193-213, doi:10.1038/nprot.2016.009 (2016).
64 Jardine, J. *et al.* Rational HIV immunogen design to target specific germline B cell receptors. *Science* **340**, 711-716, doi:10.1126/science.1234150 (2013).
65 Bar-On, Y. M., Flamholz, A., Phillips, R. & Milo, R. SARS-CoV-2 (COVID-19) by the numbers. *Elife* **9**, doi:10.7554/eLife.57309 (2020).
66 Wu, Y. *et al.* A noncompeting pair of human neutralizing antibodies block COVID-19 virus binding to its receptor ACE2. *Science* **368**, 1274-1278, doi:10.1126/science.abc2241 (2020).
67 Hauser, B. M. *et al.* Engineered receptor binding domain immunogens elicit pan-sarbecovirus neutralizing antibodies outside the receptor binding motif. *bioRxiv*, doi:10.1101/2020.12.07.415216 (2021).
68 Lingwood, D. *et al.* Structural and genetic basis for development of broadly neutralizing influenza antibodies. *Nature* **489**, 566-570, doi:10.1038/nature11371 (2012).
69 Sangesland, M. *et al.* Germline-Encoded Affinity for Cognate Antigen Enables Vaccine Amplification of a Human Broadly Neutralizing Response against Influenza Virus. *Immunity* **51**, 735-749 e738, doi:10.1016/j.immuni.2019.09.001 (2019).
70 Saunders, K. O. *et al.* Targeted selection of HIV-specific antibody mutations by engineering B cell maturation. *Science* **366**, doi:10.1126/science.aay7199 (2019).
71 McGuire, A. T. *et al.* Engineering HIV envelope protein to activate germline B cell receptors of broadly neutralizing anti-CD4 binding site antibodies. *J Exp Med* **210**, 655-663, doi:10.1084/jem.20122824 (2013).
72 Corbett, K. S. *et al.* Design of Nanoparticulate Group 2 Influenza Virus Hemagglutinin Stem Antigens That Activate Unmutated Ancestor B Cell Receptors of Broadly Neutralizing Antibody Lineages. *mBio* **10**, doi:10.1128/mBio.02810-18 (2019).
73 Ronsard, L. *et al.* Engineering an Antibody V Gene-Selective Vaccine. *Front Immunol* **12**, 730471, doi:10.3389/fimmu.2021.730471 (2021).
74 Voss, J. E. *et al.* Reprogramming the antigen specificity of B cells using genome-editing technologies. *Elife* **8**, doi:10.7554/eLife.42995 (2019).
75 Garcia-Beltran, W. F. *et al.* COVID-19-neutralizing antibodies predict disease severity and survival. *Cell* **184**, 476-488 e411, doi:10.1016/j.cell.2020.12.015 (2021).
76 Garcia-Beltran, W. F. *et al.* Multiple SARS-CoV-2 variants escape neutralization by vaccine-induced humoral immunity. *Cell* **184**, 2523, doi:10.1016/j.cell.2021.04.006 (2021).
77 Hauser, B. M. *et al.* Cross-reactive SARS-CoV-2 epitope targeted across donors informs immunogen design. *Cell Rep Med* **3**, 100834, doi:10.1016/j.xcrm.2022.100834 (2022).
78 Mombaerts, P. *et al.* Mutations in T-cell antigen receptor genes alpha and beta block thymocyte development at different stages. *Nature* **360**, 225-231, doi:10.1038/360225a0 (1992).
79 Correia, B. E. *et al.* Proof of principle for epitope-focused vaccine design. *Nature* **507**, 201-206, doi:10.1038/nature12966 (2014).
80 Schiepers, A. *et al.* Molecular fate-mapping of serum antibody responses to repeat immunization. *Nature* **615**, 482-489, doi:10.1038/s41586-023-05715-3 (2023).
81 Rappuoli, R. Glycoconjugate vaccines: principles and mechanisms. *Sci Transl Med* **10**, doi:10.1126/scitranslmed.aat4615 (2018).
82 Schumann, B. *et al.* A semisynthetic Streptococcus pneumoniae serotype 8 glycoconjugate vaccine. *Sci Transl Med* **9**, doi:10.1126/scitranslmed.aaf5347 (2017).

83 Tian, J. H. *et al.* SARS-CoV-2 spike glycoprotein vaccine candidate NVX-CoV2373 immunogenicity in baboons and protection in mice. *Nat Commun* **12**, 372, doi:10.1038/s41467-020-20653-8 (2021).
84 Heath, P. T. *et al.* Safety and Efficacy of NVX-CoV2373 Covid-19 Vaccine. *N Engl J Med* **385**, 1172-1183, doi:10.1056/NEJMoa2107659 (2021).
85 Huckriede, A., Bungener, L., Daemen, T. & Wilschut, J. Influenza virosomes in vaccine development. *Methods Enzymol* **373**, 74-91, doi:10.1016/S0076-6879(03)73005-5 (2003).
86 Morein, B., Sundquist, B., Hoglund, S., Dalsgaard, K. & Osterhaus, A. Iscom, a novel structure for antigenic presentation of membrane proteins from enveloped viruses. *Nature* **308**, 457-460, doi:10.1038/308457a0 (1984).
87 Tokatlian, T. *et al.* Innate immune recognition of glycans targets HIV nanoparticle immunogens to germinal centers. *Science* **363**, 649-654, doi:10.1126/science.aat9120 (2019).
88 Tam, H. H. *et al.* Sustained antigen availability during germinal center initiation enhances antibody responses to vaccination. *Proc Natl Acad Sci U S A* **113**, E6639-E6648, doi:10.1073/pnas.1606050113 (2016).
89 Aung, A. *et al.* Low protease activity in B cell follicles promotes retention of intact antigens after immunization. *Science* **379**, eabn8934, doi:10.1126/science.abn8934 (2023).
90 Wamhoff, E. C. *et al.* Controlling Nuclease Degradation of Wireframe DNA Origami with Minor Groove Binders. *ACS Nano*, doi:10.1021/acsnano.1c11575 (2022).
91 Chandrasekaran, A. R. Nuclease resistance of DNA nanostructures. *Nat Rev Chem* **5**, 225-239, doi:10.1038/s41570-021-00251-y (2021).
92 Lee, J. H. *et al.* Long-primed germinal centres with enduring affinity maturation and clonal migration (vol 609, pg 998, 2022). *Nature*, doi:10.1038/s41586-023-05741-1 (2023).
93 Liu, S. *et al.* A DNA nanodevice-based vaccine for cancer immunotherapy. *Nat Mater* **20**, 421-430, doi:10.1038/s41563-020-0793-6 (2021).
94 Du, R. R. *et al.* Innate Immune Stimulation Using 3D Wireframe DNA Origami. *ACS Nano* **16**, 20340-20352, doi:10.1021/acsnano.2c06275 (2022).
95 Comberlato, A., Koga, M. M., Nussing, S., Parish, I. A. & Bastings, M. M. C. Spatially Controlled Activation of Toll-like Receptor 9 with DNA-Based Nanomaterials. *Nano Lett* **22**, 2506-2513, doi:10.1021/acs.nanolett.2c00275 (2022).
96 Dobrovolskaia, M. A. & Bathe, M. Opportunities and challenges for the clinical translation of structured DNA assemblies as gene therapeutic delivery and vaccine vectors. *Wiley Interdiscip Rev Nanomed Nanobiotechnol* **13**, e1657, doi:10.1002/wnan.1657 (2021).